Nonradiative recombination at threading dislocations in 4H-SiC epilayers studied by micro-photoluminescence mapping

Feng, Gan; Suda, Jun; Kimoto, Tsunenobu

Nonradiative recombination at threading dislocations in 4H-SiC epilayers studied by micro-photoluminescence mapping

Gan Feng, Jun Suda, and Tsunenobu Kimoto

Citation: J. Appl. Phys. **110**, 033525 (2011); doi: 10.1063/1.3622336
View online: http://dx.doi.org/10.1063/1.3622336
View Table of Contents: http://jap.aip.org/resource/1/JAPIAU/v110/i3
Published by the American Institute of Physics.

JOURNAL OF APPLIED PHYSICS **110**, 033525 (2011)

Nonradiative recombination at threading dislocations in 4H-SiC epilayers studied by micro-photoluminescence mapping

Gan Feng,[1,a)] Jun Suda,[1] and Tsunenobu Kimoto[1,2]
[1]*Department of Electronic Science and Engineering, Kyoto University, Katsura, Nishikyo, Kyoto 615-8510, Japan*
[2]*Photonics and Electronics Science and Engineering Center (PESEC), Kyoto University, Katsura, Nishikyo, Kyoto 615-8510, Japan*

(Received 17 May 2011; accepted 4 July 2011; published online 9 August 2011)

Threading dislocations (TDs) in 4H-SiC epilayers have been investigated by means of micro-photoluminescence (μ-PL) mapping at room temperature. Enhanced nonradiative recombination at TDs was confirmed experimentally, resulting in a reduced local PL emission intensity in the μ-PL intensity map performed at 390 nm (near band-edge emission). The behavior of nonradiative recombination at TDs depends on the dislocation type: the screw type of TDs shows stronger effect on the nonradiative recombination activity than the edge type, evidencing a larger local reduction of PL emission intensity. Furthermore, the contrast of TDs in the μ-PL intensity map greatly depends on the carrier lifetimes of the 4H-SiC epilayers. Lifetimes longer than 0.5 μs are essential to obtain a discernible contrast for the individual TDs. © *2011 American Institute of Physics*. [doi:10.1063/1.3622336]

I. INTRODUCTION

Although the predominance of silicon carbide (SiC) high-power devices is becoming realistic, devices made from SiC are still facing various issues related to defects nucleated in the substrates or epilayers. Dislocations are a common type of electrically active defects existing in SiC crystals with a typical density of up to $\sim 10^4$ cm^{-2}. They introduce a large number of carrier recombination centers into SiC materials, which effectively reduce the local density of free carriers upon external excitation. Dislocations can also act as carrier generation centers, leading to the increase of leakage current.[1–3] Furthermore, dislocations are more likely to have impurity atoms aggregated or segregated around them.[4] The influence of dislocations on the performance of bipolar and Schottky devices in SiC has been documented.[1–3,5,6]

Direct evidence for enhanced non-radiative recombination occurring at dislocations in SiC was obtained by recording micrographs using photoluminescence (PL) signals to give images.[7–10] In such micrographs, the individual threading dislocations (TDs), including screw and edge types, appear as dark spots, while basal plane dislocations (BPDs) show a large discernable contrast shape under the strong excitation. Similar micrographs were also obtained from 4H-SiC by using the electron beam induced current (EBIC) signals.[11–13] For all of these characterization techniques, the dark spots were correlated with TDs rigorously by comparing the dark spots with etch pits of TDs in micrographs obtained from the same specimen areas.[10–13] Although preliminary investigations have also pointed out that the screw type TDs (TSDs) are more effective in acting as non-radiative recombination centers than the edge type TDs (TEDs), there is still a lack of further experimental evidences and of a comprehensive physical model to reveal the carrier recombination behaviors at TSDs and TEDs.

One of the reasons for this limited amount of experimental works on this topic is the relatively short carrier lifetimes in the as-grown 4H-SiC epilayers, typically ~ 1 μs or less. The short carrier lifetimes indicate the high density of point defects, deep level traps, in 4H-SiC. These deep levels compete with dislocations as the carrier recombination centers and are predominant over the influence of TDs. The $Z_{1/2}$ center[14] and $EH_{6/7}$ center[15] are dominant deep levels in as-grown n-type 4H-SiC epilayers, and the $Z_{1/2}$ center has been identified as a major lifetime killer.[16,17] Since the $Z_{1/2}$ concentration can be modified by post-growth processes, the lifetime of n-type 4H-SiC epilayers can be intentionally controlled.[17–21]

In this work, we intended to improve the carrier lifetimes of thick n-type 4H-SiC epilayers by using the two-step thermal treatment, namely thermal oxidation and subsequent inert gas (Ar) annealing at high temperature.[21] Furthermore, low-energy electron irradiation was carried out to selectively reduce the carrier lifetimes within the sample.[17] The nonradiative recombination behaviors near TSDs and TEDs and their dependence on the carrier lifetimes were investigated by using a micro-photoluminescence (μ-PL) mapping method, which has been demonstrated to be a powerful technique for non-destructive studying of crystalline defects in 4H-SiC epilayers.[7,22–25] The mechanism of carrier recombination near TDs is also discussed.

II. EXPERIMENTAL

4H-SiC epilayers with the thickness of 50-80 μm were grown on 8° off-axis 4H-SiC(0001) n^+-substrates with a doping concentration of (5-6) $\times 10^{18}$ cm^{-3} by horizontal hot-wall chemical vapor deposition in a SiH_4-C_3H_8-H_2 system.[26] Epitaxial growth was performed at 1650 °C with a reactor pressure of 30 Torr and the C/Si ratio of 1.2. The growth rate was 50-80 μm/h. The epilayers were intentionally doped with

a)Author to whom correspondence should be addressed. Electronic mail: gfeng@semicon.kuee.kyoto-u.ac.jp.

nitrogen donors to 1×10^{15} cm^{-3}. The carrier lifetime of as-grown epilayers was modulated by post-growth processes. To improve the carrier lifetime, thermal oxidation was firstly carried out in dry O_2 ambience at 1300 °C for 5 h. After the oxidation, the formed oxide was removed by hydrofluoric acid etching, and the subsequent annealing in Ar was performed at 1550 °C for 30 min.[21] Low-energy electron irradiation with different fluences was carried out to reduce the carrier lifetimes of the samples.[17] Electron irradiation was performed at an energy of 160 keV without intentional sample heating to introduce deep levels. The electron-irradiated sample was then annealed in Ar at 950 °C for 30 min. The carrier lifetimes of as-grown and post-treated 4H-SiC epilayers were measured by differential microwave photoconductance decay (μ-PCD) at room temperature. An yttrium lithium fluoride-third harmonic generation laser ($\lambda = 349$ nm) was used as an excitation source. The photon density irradiated onto the sample surface was 1×10^{14} cm^{-2}, which leads to a high injection level of mid 10^{15}–10^{16} cm^{-3}.

μ-PL intensity mapping was performed at room temperature on the samples.[27] PL was excited by the 25 mW, 325 nm line of a He-Cd laser, dispersed with a grating monochromator, and detected by a photomultiplier. The penetration depth of the 325 nm laser is only ~8 μm in 4H-SiC,[28] much shorter than the thickness of the epilayers. The set-up can acquire data in a single wavelength mode (μ-PL intensity mapping mode) or in a full spectral scanning mode (PL spectroscopy mode) with the spectral resolution of 1 nm. The high lateral spacial resolution in our μ-PL mapping system, 0.5 μm, allows us to reveal individual TDs in the 4H-SiC epilayers and to study their characteristics. The schematic configuration of μ-PL intensity contrast measurements near a TD is presented in Fig. 1 (the detail is described in the discussion part.). The sample surface is scanned by a laser beam probe, of which diameter is focused to about 0.8 μm by using a lens, and the PL signals are also collected through the lens. Molten potassium hydroxide (KOH) etching was performed at 480 °C for 5~10 min after μ-PL mapping measurements on the 4H-SiC epilayers. Nomarski microscopy was utilized to obtain photomicrographs of the etched 4H-SiC surface at the same location where the μ-PL intensity mapping was performed.

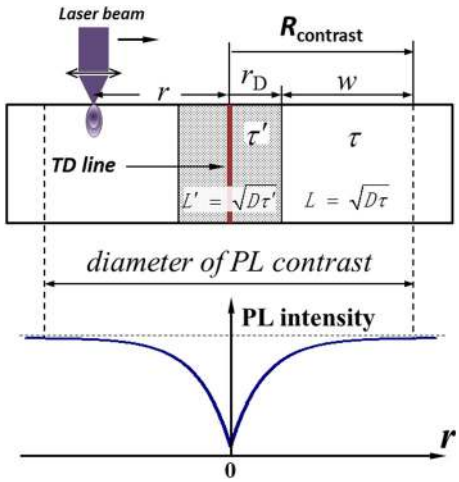

FIG. 1. (Color online) Schematic configuration of μ-PL contrast measurements at a threading dislocation.

III. RESULTS AND DISCUSSIONS

Figure 2(a) shows the μ-PL intensity mapping at 390 nm (near band-edge emission of 4H-SiC) for a 72 μm-thick 4H-SiC epilayer after the two-step thermal treatment. The carrier lifetime of the sample is approximately 5 μs, as determined by μ-PCD measurement. Three circular areas with reduced PL emission intensity in contrast to the matrix can be clearly observed. The dark contrast of the three circular areas in the μ-PL intensity map means that there is an

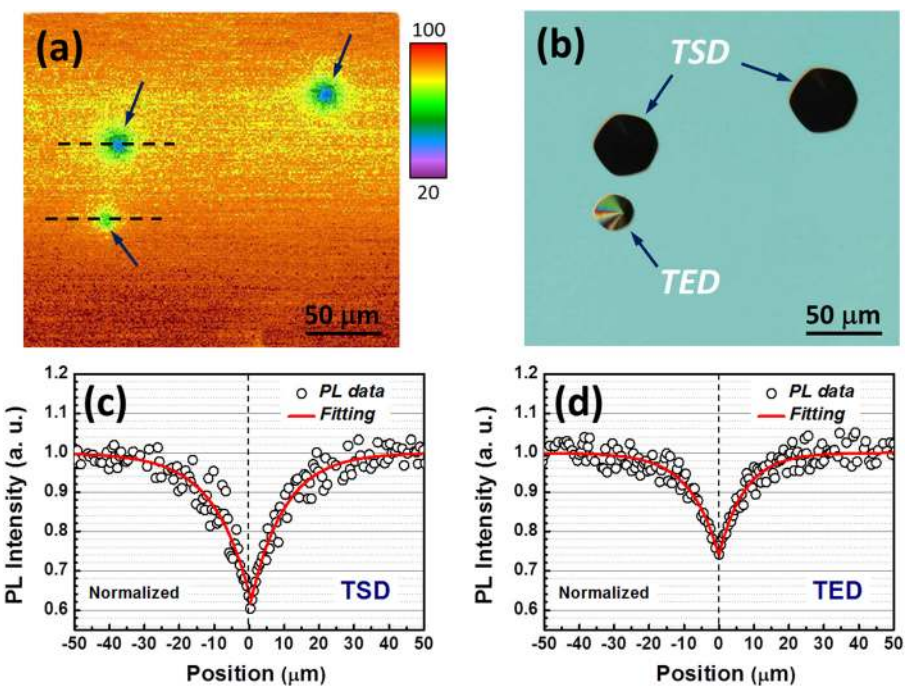

FIG. 2. (Color online) (a) μ-PL intensity mapping at 390 nm for a 72-μm-thick 4H-SiC epilayer after two-step thermal treatment. (b) Surface morphology after KOH etching (the same location). (c) PL intensity profile around a TSD shown in (a). (d) PL intensity profile around a TED shown in (a).

enhanced nonradiative recombination occurring at these positions. Among these three circular areas, two of them show a larger size than the other one. Figure 2(b) shows the optical microscopy image of the sample surface at the same location after KOH etching. Three TDs are revealed by characteristic etch pit shapes in the image. It can be seen from Figs. 2(a) and 2(b) that there is a one-to-one correlation between the circular areas, with reduced local PL intensity in the μ-PL map with TDs. That is to say, the TDs act as the enhanced nonradiative recombination centers in the sample. Furthermore, TSDs exhibit larger and deeper etch pits than the TEDs, due to the larger Burgers′ vector (the strain field), as shown in Fig. 2(b). An analogous effect was also observed in the μ-PL intensity map.

A TD contrast profile, i.e., the line scan over the TD, is given by

$$C(\mathrm{r}) = \frac{I(\mathrm{r}) - I_{matrix}}{I_{matrix}} \times 100(\%),$$

where r is the lateral beam position relative to the TD line and I_{matrix} is the matrix signal far away from it. Usually, the central value $c(0)$ is denoted as "the maximum contrast value, C_{max}," irrespective of its sign (here defined negative for a dark image contrast). Figures 2(c) and 2(d) show the profiles of PL intensities around a TSD and a TED along the dashed lines in Fig. 2(a), respectively. The C_{max} of TSD defined by Eq. (1) is 40%, larger than that of TED (26%). The large C_{max} of TSDs in the μ-PL intensity map indicates a stronger nonradiative recombination activity at TSDs than that at TEDs, being consistent with previous EBIC′s results.[13] This gives the possibility to distinguish the TSDs and TEDs nondestructively by μ-PL mapping, even at room temperature.

For comprehensive studies on the formation of the defect contrast from TDs, it is necessary to take account of the intrinsic nature of dislocation recombination. In general, defects are supposed to change the local recombination properties of the crystals. A dislocation in a semiconductor is generally charged, which induces a band bending in its neighborhood. Hence, a potential barrier for majority carriers is formed across a space-charge region, which causes minority carriers to drift toward the dislocation and significantly enhances their recombination. Beyond this core effect, the dislocation strain field is also responsible for a band bending. Dislocations can be phenomenologically described by a cylindrical region of radius r_{D}, where the carrier lifetime τ' differs (it is generally reduced) from the bulk value τ because of dislocation-induced enhancement of the recombination probability, as shown in Fig. 1. The radius r_{D} of the dislocation cylinder can be inferred as the extension of the core region, strain field, or the space charge region of a charged dislocation. Within r_{D}, the carrier has a reduced diffusion length, $L' = \sqrt{D \cdot \tau'}$, where D is the diffusion constant. The r_{D} and L' are dependent on the type of dislocations. Furthermore, the enhanced carrier recombination rate makes the dislocation cylinder act as a deep drain, attracting carriers in the surrounding region and expanding the area of dislocation contrast in μ-PL mapping. This is considered by introduction of a second region to interpret the dislocation contrast. The second region is a diffusion-limited region with the bulk diffusion length $L = \sqrt{D \cdot \tau}$. The width of this diffusion-limited region, w, is determined by two factors: the carrier recombination rate at the r_{D} (the boundary effect) and the bulk carrier diffusion length, L. The former factor is dependent on the type of TDs, while the latter is not. Taking account of indirect band-gap of 4H-SiC, it is reasonable to propose that the value of w must be much larger than r_{D}, which is expected to be below ~ 0.5 μm. Consequently, the diameter of the TDs contrast, $2R_{\mathrm{contrast}} = 2(r_{\mathrm{D}} + w)$, is determined by both the carrier recombination rate within the dislocation cylinder region (the maximum contrast of TDs) and the bulk carrier recombination rate.

To accurately fit the intensity profiles near the TDs, an appropriate physical model of carrier generation function, recombination process, and PL collection coefficients is required. Here, to simplify the simulation process, a simple decay formula was employed to fit the experimental data:

$$I(\mathrm{r}) = I_{matrix} - I_D \exp\left(-\frac{r}{L_{eff}}\right),$$

where I_{D} is the PL intensity reduction (depth) at the TD line ($r = 0$). In the μ-PL map, L' and L cannot be determined separately, but form together an "effective diffusion length (L_{eff})" of TDs. The fitting results are shown by the solid curves in Figs. 2(c) and 2(d). The effective diffusion length near the TSD is approximately 10 μm, while that of TED is about 9 μm. The small difference of the effective diffusion length between TSD and TED indicates that the diffusion-limited region is the dominant part in R_{contrast}, being consistent with the above discussion. The result also indicates that the bulk carrier recombination plays a great role in the interpretation of the PL contrast of TDs.

There are two stages before the radiation recombination of excess carriers: the first is the carrier generation process and the second is the carrier diffusion process. The excess carriers are mainly concentrated in the central region of the incident laser beam, for example, below 0.8 μm in our case. Then the excess carriers randomly walk away from the source point by diffusion. However, if there are lots of deep levels existing in the sample, the carriers will be captured by these traps before they approach the TDs. This means that the dark area of a TD contrast ($\pi R^2_{contrast}$) shrinks due to the deep levels in the sample. Figure 3 schematically shows the

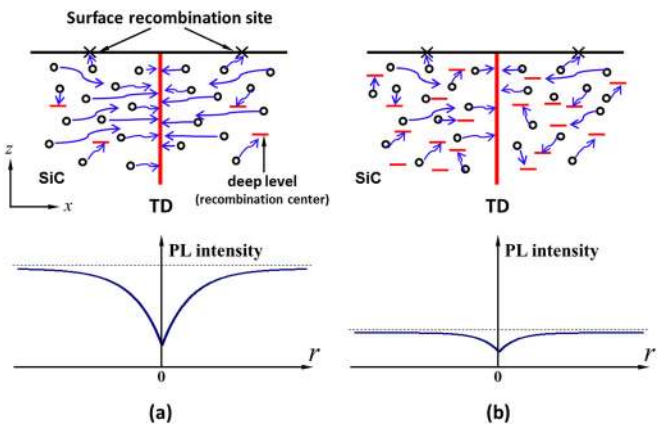

FIG. 3. (Color online) Schematic representation of the carrier recombination around a TD in the cases of: (a) low trap concentration (long bulk lifetime) and (b) high trap concentration (short bulk lifetime).

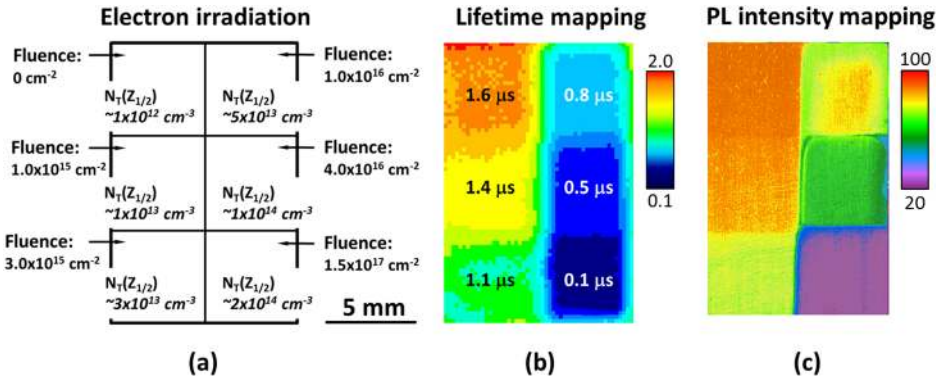

FIG. 4. (Color online) (a) Map of the fluence of electron irradiation and $Z_{1/2}$ concentration in the irradiated sample. (b) Map of carrier lifetimes in the irradiated sample. (c) μ-PL intensity mapping at 390 nm of the sample.

impact of deep levels on the recombination behavior of carriers around a TD. In the case of low deep-level concentration shown in Fig. 3(a), the carriers can diffuse over long distances without being trapped. Most carriers can migrate to the TD, even if they are generated far from it, resulting in a large dark area of $\pi R^2_{contrast}$ and also a strong contrast of TDs in the μ–PL intensity map. This situation may be preferable to distinguish TSDs and TEDs in μ–PL mapping by comparing the sizes of their dark areas and the values of C_{max}. With increasing the concentration of deep levels, more and more carriers will be trapped by deep levels, making the dark area of $\pi R^2_{contrast}$ shrink due to the decrease of the bulk diffusion length. When the deep-level concentration is very high, as shown in Fig. 3(b), strong carrier recombination occurs at the deep levels instead of at TDs, and the contrast of TDs becomes weak, making it difficult to distinguish TSDs and TEDs. In the worst case (very high deep-level concentration), there will be no discernible contrast for the TDs due to the significant recombination at deep levels before reaching TDs. The concentration of deep levels is linked to the carrier lifetime of samples. Consequently, the profile of TDs in the μ-PL intensity map might greatly depend on the carrier lifetime of epilayers.

Since the $Z_{1/2}$ concentration, the dominant lifetime killer in n-type 4H-SiC epilayers, can be selectively increased by low-energy electron irradiation, the lifetime can be intentionally controlled.[17] In this work, electron irradiation with an energy of 160 keV was performed to a 50 μm-thick as-grown n-type epilayer. The maps for the fluence of electron irradiation and of the $Z_{1/2}$ concentration in the irradiated epilayer are schematically illustrated in Fig. 4(a). The carrier lifetimes of the irradiated sample were measured by μ-PCD with a spatial resolution of 200 μm, as shown in Fig. 4(b). A higher fluence results in the shorter carrier lifetime, as expected. The carrier lifetime of the sample was locally divided into six regions, with the decreasing values corresponding to the electron fluences as 1.6, 1.4, 1.1, 0.8, 0.5, and 0.1 μs, respectively. μ-PL mapping at 390 nm was firstly performed on the whole area of the electron-irradiated sample with a scan step of 10 μm (in the low-resolution mode), as shown in Fig. 4(c). The PL intensity is reduced in the irradiated region, being consistent with the reduction of carrier lifetime.

The μ-PL mapping with a scan step of 0.5 μm (in the high-resolution mode) was then performed at each region to reveal the effects of carrier lifetimes on the non-radiative recombination behavior at TDs, as shown in Fig. 5. It is evident that, by reducing the carrier lifetime, the circular area of TDs in the μ-PL map becomes small and the contrast becomes weak. For the regions with a lifetime longer than 0.5 μs (Figs. 5(a)–5(d)), the contrast for individual TDs can be clearly observed, while, when the carrier lifetime is below 0.5 μs (see Fig. 5(e) and 5(f)), the contrast of TDs becomes too faint to be clearly identified.

Figure 6(a) shows the values of C_{max} for TSDs and TEDs as a function of the carrier lifetime. When the carrier lifetime decreases to 0.1 μs, it is difficult to fit the data due to the presence of noise, resulting in a similar contrast of $\sim$15% for both TSDs and TEDs. It is obvious that the value of C_{max} increases with increasing the carrier lifetime for both TSDs and TEDs. TSDs always show a larger value of C_{max} compared with TEDs, and the PL contrast between TSDs and TEDs also increases with increasing the carrier lifetime. The effective diffusion lengths (L_{eff} in Eq. (2)) near TSDs and TEDs as a function of the carrier lifetime are revealed in Fig. 6(b). For carrier lifetimes below 1.1 μs, the effective diffusion lengths of TSDs and TEDs show similar values. Noticeable differences in the effective diffusion length between TSDs and TEDs can be obtained for carrier

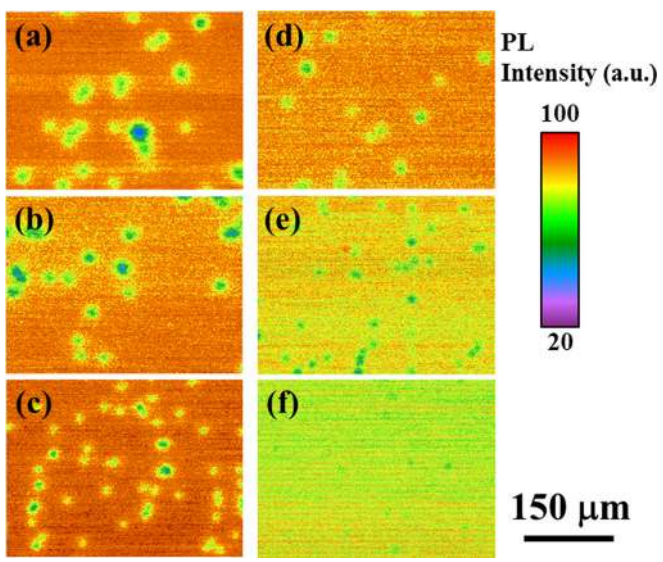

FIG. 5. (Color online) μ-PL intensity mapping images taken at the sample regions with various carrier lifetimes: (a) 1.6 μs, (b) 1.4 μs, (c) 1.1 μs, (d) 0.8 μs, (e) 0.5 μs, and (f) 0.1 μs.

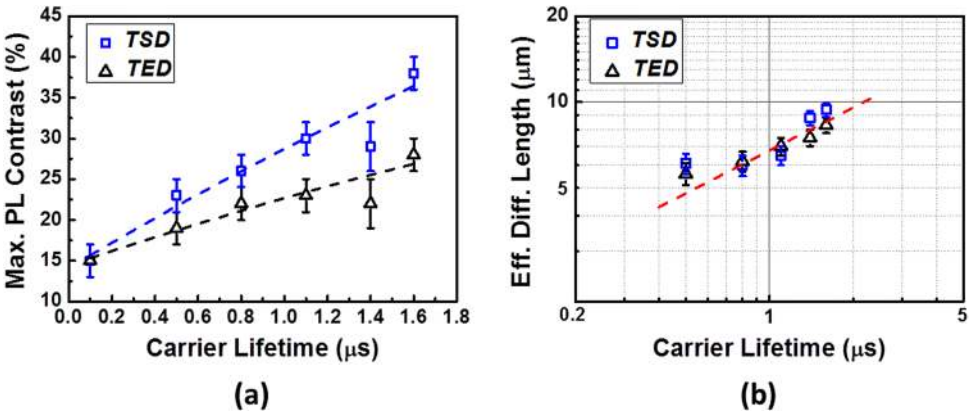

FIG. 6. (Color online) (a) Maximum PL contrast (C_{max}) of TDs as a function of the carrier lifetime. (b) Logarithmic plot of the effective diffusion length of TDs as a function of the carrier lifetime.

lifetimes longer than, for example, 1.4 μs. It should be noted that Fig. 6(b) is plotted in a *log-log* scale. The dependence of effective diffusion length on carrier lifetime shows a slope of approximately 0.5 for both TSDs and TEDs (see the dashed line in Fig. 6(b)). This means that the diffusion-limit region is dominant in forming the dark area of TDs in μ-PL mapping for the samples with relatively long carrier lifetimes. The observed results are well-consistent with the discussion mentioned above using Fig. 3. Our data indicate that longer carrier lifetimes are crucial for the nondestructive visualization of individual TDs and to distinguish TSDs and TEDs in 4H-SiC epilayers by μ-PL mapping. If the carrier lifetimes of the samples are shorter than 0.5 μs, discernable contrast cannot be obtained for the individual TDs in the μ-PL intensity map. Furthermore, the surface recombination must also cause reduction of TD's contrast and the shrinkage of the effective diffusion length in the μ-PL intensity map, which needs further investigation to propose a complete physical model.

IV. CONCLUSION

μ-PL intensity mapping was performed to characterize the local nonradiative recombination at individual TDs in 4H-SiC epilayer. The results of the μ-PL intensity mapping were compared with the post-decoration etch photomicrographs. The one-to-one correspondence between the dislocations and the μ-PL mapping contrast has been obtained. It was shown that TSDs have a more pronounced impact on the nonradiative recombination activity than TEDs. The contrast of TDs is enhanced by increasing the carrier lifetime. Carrier lifetimes longer than 0.5 μs are necessary to obtain a clear contrast pattern for the individual TDs.

ACKNOWLEDGMENTS

This work was supported by the Funding Program for World-Leading Innovative R&D on Science and Technology (FIRST Program) and a Grant-in-Aid for Scientific Research (21226008) from the Japan Society for the Promotion of Science.

[1]P. G. Neudeck, W. Huang, and M. Dudley, IEEE Trans. Electron Devices **46**, 478 (1999).
[2]Q. Wahab, A. Ellison, A. Henry, E. Janzen, C. Hallin, J. DiPersio, and R. Martinez, Appl. Phys. Lett. **76**, 2725 (2000).
[3]H. Fujiwara, M. Konishi, T. Ohnishi, T. Nakamura, K. Hamada, T. Katsuno, Y. Watanabe, T. Endo, T. Yamamoto, K. Tsuruta, and S. Onda, Mater. Sci. Forum **679–680**, 694 (2011).
[4]F. Bernardini and L. Colombo, Phys. Rev. B **72**, 085215 (2005).
[5]T. Kimoto, N. Miyamoto, and H. Matsunami, IEEE Trans. Electron Devices **46**, 471 (1999).
[6]J. P. Bergman, H. Lendenmann, P. A. Nilsson, U. Lendefelt, and P. Skytt, Mater. Sci. Forum **353–356**, 299 (2001).
[7]M. Tajima, E. Higashi, T. Hayashi, H. Kinoshita, and H. Shiomi, Appl. Phys. Lett. **86**, 061914 (2005).
[8]I. Kamata, H. Tsuchida, T. Miyanagi, and T. Nakamura, Mater. Sci. Forum **527–529**, 415 (2005).
[9]R. E. Stahlbush, K. X. Liu, Q. Zhang, and J. J. Sumakeris, Mater. Sci. Forum **556–557**, 295 (2007).
[10]G. Feng, J. Suda, and T. Kimoto, Jpn. J. Appl. Phys. **49**, 090201 (2010).
[11]Y. Yanagisawa, T. Hatayama, H. Yano, Y. Uraoka, and T. Fuyuki, Mater. Sci. Forum **527–529**, 423 (2006).
[12]B. Chen, J. Chen, T. Sekiguchi, A. Kinoshita, H. Matsuhata, H. Yamaguchi, I. Nagai, and H. Okumura, J. Mater. Sci.: Mater. Electron. **19**, S219 (2008).
[13]S. I. Maximenko, J. A. Freitas, R. L. Myers-Ward, K. K. Lew, B. L. VanMil, C. R. Eddy, D. K. Gaskill, P. G. Muzykov, and T. S. Sudarshan, J. Appl. Phys. **108**, 013708 (2010).
[14]T. Dalibor, G. Pensl, H. Matsunami, T. Kimoto, W. J. Choyke, A. Schöner, and N. Nordell, Phys. Status Solidi A **162**, 199 (1997).
[15]C. Hemmingsson, N. T. Son, O. Kordina, J. P. Bergman, E. Janzén, J. L. Lindström, S. Savage, and N. Nordell, J. Appl. Phys. **81**, 6155 (1997).
[16]P. B. Klein, J. Appl. Phys. **103**, 033702 (2008).
[17]K. Danno, D. Nakamura, and T. Kimoto, Appl. Phys. Lett. **90**, 202109 (2007).
[18]L. Storasta and H. Tsuchida, Appl. Phys. Lett. **90**, 062116 (2007).
[19]L. Storasta, H. Tsuchida, T. Miyazawa, and T. Ohshima, J. Appl. Phys. **103**, 013705 (2008).
[20]T. Hiyoshi and T. Kimoto, Appl. Phys. Express **2**, 041101 (2009).
[21]T. Hiyoshi and T. Kimoto, Appl. Phys. Express **2**, 091101 (2009).
[22]M. Tajima, E. Higashi, T. Hyashi, H. Kinoshita, and H. Shiomi, Mater. Sci. Forum **527–529**, 711 (2006).
[23]J. Camassel and S. Juillaguet, J. Phys. D: Appl. Phys. **40**, 6264 (2007).
[24]G. Feng, J. Suda, and T. Kimoto, Appl. Phys. Lett. **92**, 221906 (2008).
[25]J. Hennessy and T. Ryan, Mater. Sci. Forum **556**, 383 (2007).
[26]T. Kimoto, S. Nakazawa, K. Hashimoto, and H. Matsunami, Appl. Phys. Lett. **79**, 2761 (2001).
[27]G. Feng, J. Suda, and T. Kimoto, Appl. Phys. Lett. **94**, 091910 (2009).
[28]S. G. Sridhara, R. P. Devaty, and W. J. Choyke, J. Appl. Phys. **84**, 2963 (1998).